OPTIMAL CONTROL APPLICATIONS AND METHODS
Optim. Control Appl. Meth. 2014; **35**:1–20
Published online 12 September 2012 in Wiley Online Library (wileyonlinelibrary.com). DOI: 10.1002/oca.2049

Nonlinear model predictive control strategy for low thrust spacecraft missions

Joseph A. Starek*,† and Ilya V. Kolmanovsky

Department of Aerospace Engineering, University of Michigan, Ann Arbor, MI 48109-2140, USA

SUMMARY

In this paper, two nonlinear model predictive control (MPC) strategies are applied to solve a low thrust interplanetary rendezvous problem. Each employs a unique, nonclassical parameterization of the control to adapt the nonlinear MPC approach to interplanetary orbital dynamics with low control authority. The approach is demonstrated numerically for a minimum-fuel Earth-to-Mars rendezvous maneuver, cast as a simplified coplanar circular orbit heliocentric transfer problem. The interplanetary transfer is accomplished by repeated solution of an optimal control problem over (i) a receding horizon with fixed number of control subintervals and (ii) a receding horizon with shrinking number of control subintervals, with a doubling strategy to maintain controllability. In both cases, the end time is left unconstrained. The performances of the nonlinear MPC strategies in terms of computation time, fuel consumption, and transfer time are compared for a constant thrust nuclear-electric propulsion system. For this example, the ability to withstand unmodeled effects and control allocation errors is verified. The second strategy, with shrinking number of control subintervals, is also shown to easily handle the more complicated bounded thrust nuclear-electric case, as well as a state-control-constrained solar-electric case. Copyright © 2012 John Wiley & Sons, Ltd.

Received 26 January 2012; Revised 5 August 2012; Accepted 7 August 2012

KEY WORDS: model predictive control; rendezvous; trajectory optimization; spacecraft; low thrust

1. INTRODUCTION

In this paper, a nonlinear model predictive control (NMPC) approach is considered for generating feedback control laws that can robustly perform low thrust spacecraft interplanetary rendezvous maneuvers. From as early as the 1960s, there have been significant developments in optimization and control applied to low thrust missions [1]. Even today, low thrust optimal control is advancing as the interest in electric propulsion grows. Recent initiatives in the use of electric propulsion for primary propulsion include the Japan Aerospace Exploration Agency Hayabusa mission, an asteroid sample return mission, and the National Aeronautics and Space Administration Dawn mission, currently in flight and, at the time of this writing,‡ using its ion engines to rendezvous with asteroid Vesta [2]. By nature of their low thrust engines, interplanetary spacecraft requires long periods of thrust time to accelerate to appropriate interplanetary or escape velocities. This inevitably subjects them to trajectory error accumulation due to unmodeled influences, including initial position and velocity errors, solar radiation pressure, gravitational perturbations, aerodynamic drag, and other error sources such as thrust mismatch and thruster misalignment. The vast majority of research thus far has focused on higher-fidelity modeling and improving open-loop optimal control

*Correspondence to: Joseph A. Starek, Department of Aerospace Engineering, University of Michigan, Ann Arbor, MI 48109-2140, USA.

†E-mail: jstarek@stanford.edu

‡http://dawn.jpl.nasa.gov/

solutions. In practice, spacecraft relying on these trajectories almost certainly require some form of ad hoc error correction to compensate for disturbance effects. The use of feedback control allows for progressive error mitigation that can rectify and prevent such errors [3]. This paper attempts to explore and implement systematic, automated approaches to trajectory correction by using MPC as opposed to the traditional individualized midcourse or terminal trajectory correction maneuvers (TCMs). MPC is selected because of its ability to achieve high performance in control problems with stringent constraints (as is the case with low thrust actuation) and its inherent robustness to disturbances/uncertainties. It is later shown that the additional cost in computation has negligible effect given the long duration of the spacecraft rendezvous maneuver. A preliminary conference version of this paper has appeared in [4].

There have been significant developments in MPC for closed-loop control of linearized dynamical systems [5, 6], and in this realm, MPC has had great success. Example spacecraft applications include proximity operations and station keeping [7–9]. Typically, however, this approach requires that the configuration space of the system remains within the proximity of an equilibrium point, which limits their applicability to certain problems (see [10] for an interesting exception, however). In particular, low thrust interplanetary spacecraft operate with highly nonlinear dynamics well removed from any equilibria and thus require a fully nonlinear treatment. This motivates the use of NMPC for attaining robust closed-loop trajectory control of low thrust spacecraft.

In this study, the approach of systematic trajectory corrections over the horizon of an optimized trajectory is explored to minimize errors in the final state vector. Specifically, a nonclassical, minimum-fuel, NMPC strategy is employed, where frequent midcourse trajectory corrections are based on reoptimizing the trajectory subject to the current state as the initial condition. The trajectory horizon is discretized into a series of control subintervals over which control laws become piecewise linear. Two novel strategies are examined for iteratively reevaluating the optimal control problem (OCP) over a receding horizon: (i) maintaining a fixed number of control subintervals and (ii) reducing the number of subintervals by one after each iteration, with a strategy to double the number when advantageous or controllability is lost. As a baseline study, the NMPC framework is applied to a class of planar, heliocentric Earth-to-Mars orbital rendezvous problems. Under a selection of low thrust nuclear-electric and solar-electric propulsion scenarios, the performance of the NMPC framework is evaluated against that of an open-loop optimal control trajectory, and the ability to converge to Mars, total fuel consumption, total transfer duration, and computation times are quantified and compared. Comparison is made with the open-loop trajectory, as opposed to another feedback strategy, to illustrate the amount of error that would normally need to be corrected by a terminal TCM.

A handful of studies has already been conducted regarding low thrust NMPC. One study of low thrust NMPC uses a direct transcription method to obtain robust closed-loop Low Earth Orbit (LEO) transfers [11]. In [12], Gao provides closed-loop low thrust trajectory guidance by minimizing mean orbital element errors using NMPC. In [13], Losa employs a direct approach to solve a parameter optimization transcription of the maneuver planning problem for geostationary satellites, applying closed-loop control using both a fixed-horizon constrained nonlinear OCP and a receding horizon problem subject to linearized orbital element equations of motion. Similar to our work, [14] considers an Earth-to-Mars transfer by using a different NMPC approach for a low thrust spacecraft, applying feedback to compensate for a 2-day thruster failure. Huang *et al.* [14] attempts to alleviate computational intensity of the problem by using a differential transformation algorithm to solve the open-loop OCP. Our paper instead focuses on inherent robustness, studying the more difficult problem of direct rendezvous with the planet, as well as examining the effects of unmodeled dynamics, and randomized off-nominal thrust magnitudes and directions. In these papers and the bulk of NMPC trajectory research, the problem of orbital transfer is primarily considered, in which the spacecraft may terminate its maneuver at any one of the infinite states along the target orbit. In the rendezvous case, the spacecraft must reach the one state along the orbit currently occupied by the target itself, which changes in time. This represents an additional and difficult-to-handle constraint, particularly in cases of very limited control authority. Our original contribution is in this study of low thrust interplanetary rendezvous with feedback and in the development of the two novel NMPC control subinterval strategies that we employ.

DOI: 10.1002/oca

The paper is organized as follows. Section 2 discusses the formulation of the OCP and outlines in detail the MPC strategies employed. Section 3 describes the equations of motion, the propulsion system models, and the perturbation models, both as seen by the spacecraft (denoted as the 'predictive' model) and as actually used for simulation (termed the 'simulation' model). Section 4 provides the numerical results of the Earth-to-Mars rendezvous study, followed by concluding remarks in Section 5.

2. MODEL PREDICTIVE CONTROL STRATEGIES

Model predictive control is a feedback law based on a repeated solution of an optimal control problem (OCP) using the current state as the initial condition. Denote the state at time $t + \tau$, predicted at time t, as $x(t + \tau|t)$. An OCP is formed to minimize a cost functional, $J = K(x(t + T_h), t + T_h) + \int_0^{T_h} L(x(t + \tau), u(t + \tau), \tau)\mathrm{d}\tau$, which is a function of the actual initial state, $x(t)$, and the predicted states and controls, $x(t + \tau|t)$, $u(t + \tau)$, over the duration of some planning period ($0 \leqslant \tau \leqslant T_h$). This OCP is solved for a finite-horizon optimal control trajectory, $u^*(t + \tau, x(t))$, that optimizes the predicted state response over the duration of the planning period. In the MPC strategy, only the initial segment of the optimal control trajectory is actually applied to the system. After implementation of the first control segment, the current state of the spacecraft is used as the initial state to update the optimization problem and planning period, and the process is repeated until convergence. This characteristic process is what gives MPC its other common names: 'receding horizon optimal control' or 'moving horizon optimal control'.

The receding horizon concept allows one to design a feedback controller on the basis of nearly any open-loop optimal control-based approach, improving its robustness and imparting it the ability to handle disturbances and mitigate error growth. Even without prior knowledge of the nature of these disturbances, one can demonstrate under appropriate assumptions that this introduction of feedback will lead to closed-loop stability and state convergence to the target [15]. Other advantages of MPC include the ability to handle pointwise-in-time state and control constraints, the incorporation of previous disturbance information, the capability to withstand time delays, and reconfiguration in the presence of degradations and failure modes [16].

2.1. Optimal control problem formulation

A restricted two-body, heliocentric Earth-to-Mars rendezvous problem is considered in which the initial positions and velocities of the spacecraft, Earth, and Mars are known, and the initial time, t_0, is given (see Figure 1). The following assumptions are made:

- The spacecraft employs a low thrust ($\sim 5 \cdot 10^{-6}$ N $-$ 0.5 N) propulsion system. [17]
- The spacecraft is modeled as a point mass (it is infinitesimal with respect to the sun, Earth, and Mars).
- The thrust vector is free to point in any direction within the orbital plane of the spacecraft.
- The Earth, Mars, and spacecraft orbital planes coincide with the ecliptic plane.
- All planets are in exact circular orbits at radii equal to their mean radii about the sun.
- The sun acts as a point mass and as a point source of light and solar pressure.
- Simulations begin in Earth's orbit about the sun at the boundary of Earth's sphere of influence—it is assumed that the spacecraft reaches this boundary with zero hyperbolic excess speed, for instance, through the propulsive force of a launch vehicle.
- Earth initially lags behind the spacecraft by a distance of $r_{\mathrm{SOI}} = r_{\mathrm{E}} \cdot (m_{\mathrm{E}}/m_{\mathrm{S}})^{2/5}$, the sphere of influence of Earth [18].

The aforementioned assumptions were made to simplify the exposition and analysis of the MPC framework to assess its applicability and benefits to orbital rendezvous problems.

The assumption of coplanar orbital transfer leads to the use of polar coordinates for the position and velocity of the spacecraft, with the most convenient location for the origin being the center of

DOI: 10.1002/oca

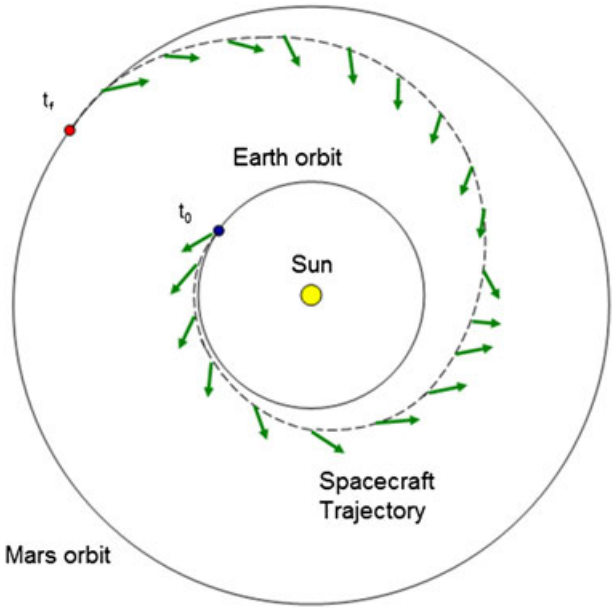

Figure 1. Schematics of a rendezvous between Earth and Mars. The arrows point in the thrust force direction.

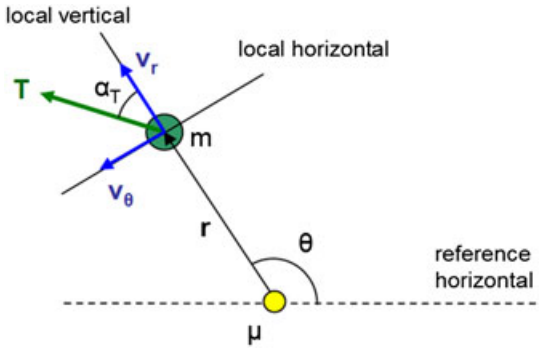

Figure 2. Illustration of spacecraft heliocentric motion and the polar coordinate frame.

the sun. In this frame (see Figure 2), the positions and velocity vectors of the spacecraft are described by

$$\boldsymbol{r} = r\hat{\boldsymbol{r}}, \tag{1}$$

$$\mathbf{v} = \dot{r}\hat{\boldsymbol{r}} + r\dot{\boldsymbol{\theta}}\hat{\boldsymbol{\theta}} = v_r\hat{\boldsymbol{r}} + v_\theta\hat{\boldsymbol{\theta}}, \tag{2}$$

where θ is the angular position of the spacecraft from a reference horizontal. Because the mass change of the spacecraft as fuel is consumed is significant, its mass must be included in the state vector. Therefore, to fully describe the system, a state vector $x = [r, \theta, v_r, v_\theta, m]$ is prescribed.

By defining our objective function as $J = K(x(t_f), t_f) + \int_0^{t_f - t_0} L(x(\tau), u(\tau), \tau)\mathrm{d}\tau$, the OCP for this Earth-to-Mars rendezvous scenario becomes

$$\begin{aligned} &\min && J \\ &\text{subject to:} && \dot{x} = f(x(t), u(t), t), \\ & && \boldsymbol{r}(t_0) = \boldsymbol{r}_0 = r_{\mathrm{E}}\hat{\boldsymbol{r}}, \end{aligned} \tag{3}$$

DOI: 10.1002/oca

$$\boldsymbol{v}(t_0) = \boldsymbol{v_0} = \sqrt{\frac{\boldsymbol{\mu}}{\boldsymbol{r_E}}}\hat{\boldsymbol{\theta}},$$

$$\theta(t_0) = \theta_E(t_0)\frac{(r_E)_{SOI}}{r_E},$$

$$m(t_0) = m_0, \tag{4}$$

$$\boldsymbol{r}(t_f) = \boldsymbol{r_M} = r_M\hat{\boldsymbol{r}},$$

$$\boldsymbol{v}(t_f) = \boldsymbol{v_M} = \sqrt{\frac{\boldsymbol{\mu}}{\boldsymbol{r_M}}}\hat{\boldsymbol{\theta}},$$

$$\theta(t_f) = \theta_M(t_f) = \theta_M(t_0) + \sqrt{\frac{\boldsymbol{\mu}}{\boldsymbol{r_M^3}}}(t_f - t_0). \tag{5}$$

The aforementioned boundary conditions ensure circular velocity at Earth (denoted by a subscript E) orbit at time t_0, circular velocity at Mars (denoted by a subscript M) at time t_f, and positional matching with Mars at time t_f. The equations of motion, $\dot{x} = f(x(t), u(t), t)$, will be summarized in Section 3.1. Note that θ_E and θ_M are not included as states because $\theta_E(t)$ and $\theta_M(t)$ can be calculated analytically from the laws of circular motion as

$$\theta_E(t) = \theta_E(t_0) + \sqrt{\frac{\boldsymbol{\mu}}{\boldsymbol{r_E^3}}}(t - t_0),$$

$$\theta_M(t) = \theta_M(t_0) + \sqrt{\frac{\boldsymbol{\mu}}{\boldsymbol{r_M^3}}}(t - t_0). \tag{6}$$

For the minimum-time OCP, the cost functional J is the time difference $t_f - t_0$, where $K = 0$, $L = 1$. For the minimum-fuel OCP, the cost functional J is the fuel expenditure $m_0 - m_f$, where $K = m_0 - m$, $L = 0$ (or, alternatively, $K = 0$, $L = -\dot{m}$). When thrust magnitude is constant and only the thrust direction is being optimized, the solution to the minimum-fuel problem coincides with that of the minimum-time problem. In what follows, the constant thrust and variable thrust cases will be examined separately.

2.2. MPC for minimum-time problems

In the case of constant thrust magnitude, the basic MPC strategy recomputes the minimum-time optimal control as a function of time as the spacecraft progresses along its trajectory. Specifically, the optimal control, $u^*(t + \tau, x(t)), 0 \leqslant \tau \leqslant S(t, x(t))$, is computed as a function of time τ given the current state of the spacecraft $x(t)$ at the time instant t. Here, $S(t, x)$ denotes the minimum time to transfer from the state x at time t to the target state x_T; that is, $S(t, x)$ is the cost-to-go in the minimum-time OCP. The computed control function is applied to the spacecraft over the time interval $t \leqslant \tau \leqslant t + \Delta t$, where $\Delta t < S(t, x(t))$, and the solution is recomputed again at the time instant $t + \Delta t$. This process of periodically recomputing the optimal control as a function of time for the current state of the spacecraft as an initial condition continues until the spacecraft reaches the target state. Such an MPC strategy can be interpreted as a form of feedback control.

If there are no disturbances or model uncertainties, then by Bellman's principle of optimality there is no difference in applying the MPC feedback or just applying the open-loop control function, $u^*(\tau, x(0)), 0 \leqslant \tau \leqslant S(0, x(0))$. There are, however, differences and advantages to recomputing the

DOI: 10.1002/oca

control along the trajectory if disturbances are present. To be specific, suppose that the equations of motion for the system with the disturbances are given by

$$\dot{x} = f(t, x, u, w), \tag{7}$$

where w denotes the disturbance and $w = 0$ corresponds to the disturbance-free case. Considering the properties of $S(t, x(t))$ as the time-to-go, it is noted that $S(t, x_T) = 0$ and $S(t, x) > 0$ if $x \neq x_T$. Under the assumption that $S(t, x)$ is continuously differentiable and satisfies the Hamilton–Jacobi–Bellman equation [19], the time rate of change of $S(t, x(t))$ along the trajectories of the disturbance-free system is

$$\dot{S} = S_t(tx) + S_x(tx) \cdot f\left(t, x, u^*(t, x), 0\right) = -1. \tag{8}$$

Consequently, $S(t, x(t)) \to 0$ and $x(t) \to x_T$ in finite time. In the case when disturbances are present and the update rate of the MPC law is sufficiently high (i.e., Δt is sufficiently small), the application of the MPC feedback approximates the application of the minimum-time feedback law, $u^*(t, x(t))$. In fact, if the minimum-time feedback law could be computed (or approximated) in closed form offline, there would not be a need for an online MPC strategy that provides a specific value, $u^*(t, x(t))$, through the numerical optimization. In the case $w \neq 0$,

$$\begin{aligned}
\dot{S} &= S_t(t, x) + S_x(t, x) f\left(t, x, u^*(t, x), w\right) \\
&= S_t(t, x) + S_x(t, x)(f\left(t, x, u^*(t, x), w\right) - f\left(t, x, u^*(t, x), 0\right)) + S_x(t, x) f\left(t, x, u^*(t, x), 0\right) \\
&= -1 + S_x(t, x)\left(f(t, x, u^*(t, x), w) - f(t, x, u^*(t, x), 0)\right).
\end{aligned} \tag{9}$$

Suppose there exists $\epsilon > 0$ such that, for all t, x such that $S(t, x) \leqslant S(0, x(0))$ and for all possible values of the bounded disturbance w,

$$S_x(t, x) \cdot \left(f(t, x, u^*(t, x), w) - f\left(t, x, u^*(t, x), 0\right)\right) \leqslant 1 - \epsilon. \tag{10}$$

This assumption is reasonable if the disturbance w is bounded and sufficiently small. Then, $\dot{S} \leqslant -\epsilon$ and $S(t, x(t)) \to 0$, $x(t) \to x_T$ in finite time despite the presence of disturbances.

Thus, in the case of constant thrust magnitude and minimum-time problems, the aforementioned analysis suggests that the MPC framework provides desirable robustness properties with respect to bounded disturbances. This illustrates theoretically, at least for the simplest case of low thrust trajectory control, the validity of using MPC to provide feedback and disturbance rejection.

2.3. Numerical strategies for computing MPC law

Several strategies can be considered for computing MPC laws. The strategies employed in this paper are tailored to a numerical optimizer that uses transcription of the OCP on the basis of a given number of control nodes (also called control subintervals) and a direct multiple-shooting approach applied to a free end-time problem. For all strategies discussed, the control is piecewise linear over the planning horizon with slope changes at subinterval endpoints, transforming the OCP of Section 2.1 into a finite-dimensional parameter optimization problem. It is noted from the numerical experience of the authors and the analysis of the previous section that the following strategies appear to have inherent robustness properties; however, a rigorous study of their disturbance rejection properties is relegated to future publications.

2.3.1. Constant number of control nodes (CNCN) strategy. In the CNCN strategy, the MPC OCP is solved with a fixed number of control nodes. In this strategy, the planning horizon is from the current time instant until the time t_f at which the spacecraft has achieved rendezvous with Mars. Rendezvous is defined as a state for which the position error to Mars is less than the radius of the

DOI: 10.1002/oca

sphere of influence (SOI) of Mars [18], $\|\boldsymbol{r} - \boldsymbol{r}_{\mathbf{M}}\| < (r_{\mathrm{SOI}})_{\mathrm{M}} = r_{\mathrm{M}} \cdot (m_{\mathrm{M}}/m_{\mathrm{S}})^{2/5}$ and the velocity error with Mars is less than 1 km/s, $\|\boldsymbol{v} - \boldsymbol{v}_{\mathbf{M}}\| < 1$ km/s, after which point we assume that a local spacecraft maneuvering controller takes over. This partitioning of the spacecraft trajectory into planetary departure, heliocentric orbital transfer, and planetary arrival is consistent with broadly used patched conic methods. Note that because the rendezvous problem is a free end-time problem, with t_f a parameter yet to be determined, the end of each planning horizon is not fixed (although time rescaling can be used to obtain an OCP with fixed time interval).

Suppose the time instants of control nodes are determined by the optimizer at each of the instants $t_0^k, t_1^k, \ldots, t_N^k$. Then, the computed numerically optimal control is applied to the spacecraft between the time t_0^k and the time of the first control node t_1^k. At time t_1^k, k is incremented, and the optimal control is recomputed assuming the same total number of control nodes. Note that the actual time instants of control nodes $t_0^{k+1}, t_1^{k+1}, \ldots, t_N^{k+1}$ can be different from $t_0^k, t_1^k, \ldots, t_N^k$. With a CNCN, as the planning horizon shrinks in length and the spacecraft progresses towards the target, the duration of each control subinterval shrinks. Thus, the effective 'sampling' frequency of the feedback loop increases as the spacecraft approaches the target planet, so that finer control corrections can take place closer to the target. Because the number of control nodes remains constant, the numerical complexity of the online optimization problem remains approximately the same for each iteration. Infinitesimally spaced control nodes are avoided by termination of the controller within a finite tolerance of the target defined by the SOI. A subtle issue that hinders computations for the CNCN strategy is that constructing an initial guess for the control trajectory based on the solution computed at the previous time instant requires interpolation, which, as the numerical experience of the authors shows, may not be accurate.

2.3.2. Shrinking number of nodes (SNN) strategy. In the SNN MPC strategy, the number of control nodes used in the planning horizon at the current time instant is reduced by one compared with the number of control nodes used in the planning horizon at the previous time instant. With this strategy, the end portion of the optimal control trajectory (the solution for all control subintervals excluding the first one) from the planning period at the previous time instant is suitable as an initial guess for the optimal control trajectory over the planning period at the current time instant. The ability to reuse the previous solution as an initialization for the next iteration not only reduces the computational effort but also ensures more stable and robust convergence. Because the number of control nodes decreases as the spacecraft progresses along the trajectory, the numerical complexity of the optimization problem decreases. The drawback of the SNN strategy is that with the decrease in the number of control nodes, the ability to make finer corrections and compensate for disturbances is lost as the spacecraft approaches the target.

2.3.3. Shrinking number of nodes with subdivision (SNNS) strategy. To avoid the loss of corrective ability that hinders SNN MPC, a further node subdivision strategy was superimposed to the SNN strategy, in which twice as many control nodes are selected if the percentage cost difference between the optimal trajectory with twice as many nodes and the optimal trajectory with the original number of nodes is less than a predefined threshold. That is to say, if doubling the number of control nodes for any given planning period results in a significantly improved solution or converges in the case that the original number of nodes does not, then the number of nodes is doubled. The number of control nodes can still decrease from one planning period to another planning period, but it may also increase if a subdivision substantially improves the solution. The term 'subdivision' refers to this doubling of the number of control nodes. Subdivision conveniently permits fore-use of the control trajectory computed at the previous time instant as an initial guess for the control trajectory at the current time instant, eliminating the need for the interpolation that hinders the CNCN strategy. To limit the computational effort and prevent unbounded expansion of the dimensions of the OCP, a limit was placed on the maximum number of subdivisions that may occur over the course of the simulation. A minimum number of control nodes was also enforced to prevent a loss of controllability.

DOI: 10.1002/oca

3. PREDICTIVE AND SIMULATION MODELS

The predictive model used for optimal control and MPC strategy, and the simulation model including orbital perturbations and disturbances, which were not accounted for in the predictive model but affected the simulated spacecraft motion, are now discussed for the numerical Earth-to-Mars rendezvous simulations that follow.

3.1. Equations of motion

The nominal model corresponds to the restricted two-body problem for spacecraft motion about the sun, where the spacecraft and sun are represented as point masses and the spacecraft mass is negligibly small in comparison with that of the sun. The equations of motion for this scenario, as described in a rotating polar frame centered at the sun (see Figure 2), are given by

$$\dot{r} = v_r,$$

$$\dot{\theta} = \frac{v_\theta}{r},$$

$$\dot{v_r} = \frac{v_\theta^2}{r} - \frac{\mu}{r^2} + \frac{T}{m}\cos\alpha_{\mathrm{T}} + \left(f_{\mathrm{perturb}}\right)_r,$$

$$\dot{v_\theta} = \frac{-v_\theta v_r}{r} + \frac{T}{m}\sin\alpha_{\mathrm{T}} + \left(f_{\mathrm{perturb}}\right)_\theta, \tag{11}$$

where the states are the distance from the sun, r, the polar angle of the spacecraft, θ, the spacecraft radial velocity component, v_r, the spacecraft tangential velocity component, v_θ, and the total spacecraft mass, m, which varies as the spacecraft expends fuel [1, 20]. The terms $\left(f_{\mathrm{perturb}}\right)_r$ and $\left(f_{\mathrm{perturb}}\right)_\theta$ are the resultant perturbing forces per unit mass in the radial and circumferential directions, respectively. These perturbing forces, used in the simulated spacecraft motion but unknown to the optimizer, consisted of third-body gravitational effects, solar radiation pressure, and control disturbances, as described in the following sections. The control models describing the thrust, T, and the final equation of motion, $\dot{m}$, are discussed next.

3.2. Propulsion models

3.2.1. Nuclear-electric propulsion model. Nuclear-electric propulsion systems rely on a nuclear power source to generate voltage potentials capable of ionizing and accelerating a working fluid. Their propulsive capability is independent of the spacecraft position in space. Following Kim [20], it is assumed that the specific impulse, I_{sp}, is constant and the propulsive thrust, T, is bounded by a maximum value $T_{\max}$, that is,

$$0 \leqslant T(t) \leqslant T_{\max}. \tag{12}$$

It can be shown from the definition of specific impulse that

$$\dot{m} = \frac{-T}{g_0 I_{\mathrm{sp}}}, \tag{13}$$

where I_{sp} is the specific impulse and g_0 is the standard acceleration due to Earth's gravity. In the special case that T is constant, that is, $T^*(t) = T_0 = \textit{constant}$, then only the thrust angle can be varying as a control. With T_0 and I_{sp} constant, the mass consumption rate of the spacecraft in this case is constant, causing the minimum-fuel and minimum-time OCP's to be exactly equivalent.

DOI: 10.1002/oca

3.2.2. Solar-electric propulsion model. Solar-electric propulsion systems depend on solar cells for conversion of solar energy to electric energy for use in ionizing and accelerating a working fluid. Because of this dependence on sunlight, the control authority of solar-electric systems varies on the basis of the distance r from the sun, thereby producing a mixed state-control constraint of the kind that can be handled by MPC. One simple method to simulate this state-dependent effect is to use a variation of the model suggested by Williams and Coverstone-Carroll and used by Kim [20, 21]:

$$0 \leqslant T \leqslant \left(b_1 + b_2 P_{\max}(r) = b_1 + b_2 P_0 \frac{a_1 r^2 + a_2 r + a_3}{r^4 (1 + a_4 r)} \right),$$

$$\dot{m} = c_1 + c_2 P(r) = c_1 + c_2 \left(\frac{T(r) - b_1}{b_2} \right), \tag{14}$$

where r is in astronomical units (AU), P_0 is the reference power corresponding to $r_0 = 1$ AU, T is the thrust, $\dot{m}$ is the fuel consumption rate, and a, b_i, and c_i are engine-specific constant parameters (see the Appendix for the list of parameters used here). It is assumed that the propulsion system may be throttled continuously from off to maximum.

3.3. Gravitational perturbations

Gravitational forces due to secondary celestial bodies were considered as additional perturbations acting on the spacecraft. These forces were considered to be much smaller than the gravitational pull of the central attractor (the sun) due to the assumptions employed in the problem scenario (as defined in Section 2.1). The gravity forces of Earth and Mars on the spacecraft are the most significant gravitational perturbations during an Earth-to-Mars interplanetary heliocentric orbital transfer. Assuming that the spacecraft begins at the boundary of the Earth's sphere of influence and ends at the boundary of Mars' sphere of influence, it follows that the gravitational forces of Earth and Mars never exceed the influence of the sun. Gravitational perturbations due to Earth and Mars can be written from Newton's law of gravity [22] as

$$(\boldsymbol{F}_{\mathbf{grav}})_i = \frac{-\mu m}{r_{\text{rel}}^2} \hat{\boldsymbol{r}}_{\mathbf{rel}} = \frac{-\mu m}{r_{\text{rel}}^3} \boldsymbol{r}_{\mathbf{rel}}, \tag{15}$$

where

$$r_{\text{rel}} = \sqrt{r^2 + r_i^2 + 2 \cdot r \cdot r_i \cdot \cos(\theta_i - \theta)}. \tag{16}$$

Here, $i = 1$ refers to Earth, and $i = 2$ refers to Mars. Also, it can be shown that

$$\boldsymbol{r}_{\mathbf{rel}} = (r - r_i \cdot \sin(\theta_i \cdot \theta))\, \hat{\boldsymbol{r}} + (-r_i \cdot \cos(\theta_i - \theta))\, \hat{\boldsymbol{\theta}}. \tag{17}$$

By approximating the orbit of the ith body attractor as an exact circular orbit about the sun, r_i is a known constant, and θ_i may be computed analytically given $\theta_i(t_0)$ and using (6). By decomposing (17) into its radial and circumferential components, substituting into (15), and summing over all perturbing bodies,

$$\left(f_{\text{grav}}\right)_r = \sum_{i=1}^{2} \frac{(F_r)_i}{m} = \sum_{i=1}^{2} \frac{\mu_i}{\left(r^2 + r_i^2 + 2 \cdot r \cdot r_i \cdot \cos(\theta_i - \theta)\right)^{3/2}} (r_i \cdot \sin(\theta_i - \theta) - r),$$

$$\left(f_{\text{grav}}\right)_\theta = \sum_{i=1}^{2} \frac{(F_\theta)_i}{m} = \sum_{i=1}^{2} \frac{\mu_i}{\left(r^2 + r_i^2 + 2 \cdot r \cdot r_i \cdot \cos(\theta_i - \theta)\right)^{3/2}} (r_i \cdot \cos(\theta_i - \theta)), \tag{18}$$

where $i = 1$ refers to Earth and $i = 2$ refers to Mars.

DOI: 10.1002/oca

3.4. Solar radiation pressure perturbations

Radiation pressure disturbances were approximated by a simplified form of the standard solar radiation pressure force model used for solar sail spacecraft. As described by Dachwald [23], the pressure associated with photons emitted by the sun is

$$P_{\text{rad}} = \frac{S}{c}, \tag{19}$$

where P is the solar radiation pressure, S is the solar radiation flux, and c is the speed of light in vacuum. By approximating the sun as a point source of light (i.e., assuming the spacecraft is sufficiently far away from the sun during its interplanetary trajectory), the solar radiation flux can be modeled using an inverse-square law, yielding

$$P_{\text{rad}}(r) = \frac{S_0}{c}\left(\frac{r_0}{r}\right)^2, \tag{20}$$

where S_0 is the mean solar radiation flux, 1368 W/m^2, at the mean Earth orbit radius $r_0 = 1$ AU. From this definition, the solar radiation force acting on the spacecraft can be found. In the ideal case in which photons transfer their momentum to the spacecraft with 100% efficiency, the solar radiation pressure force is given by

$$\boldsymbol{f}_{\mathbf{rad}} = \frac{1}{m} 2 P_{\text{rad}}(r) A\,(\boldsymbol{r}\cdot\boldsymbol{n})\,\boldsymbol{n}, \tag{21}$$

where A is the area of the solar sail spacecraft and $\boldsymbol{n}$ is the normal vector of the solar sail spacecraft [23]. For the purposes of this analysis, the spacecraft is assumed to have a constant planform area with respect to the sun–spacecraft line; thus, $A\,(\boldsymbol{r}\cdot\boldsymbol{n}) = A_{\text{s/c}}$, the projected area of the spacecraft onto the sun–spacecraft line, is constant. This assumption implies either an approximate spherical symmetry for the case of a nuclear-electric spacecraft or that an attitude control scheme is being enforced for the case of a solar-electric spacecraft such that its solar panels are always oriented normal to the sun–spacecraft line. In either case, this also implies that $\boldsymbol{n}$ is oriented along $\boldsymbol{r}$. To roughly account for imperfect reflectivity of the spacecraft exterior and/or absorption of photons from the solar arrays, an efficiency parameter $0 < \eta < 1$ is inserted into the ideal solar radiation pressure force model. This finally yields the simplified solar radiation force model:

$$\boldsymbol{f}_{\mathbf{rad}} = \frac{1}{m} 2\eta P_{\text{rad}}(r) A_{\text{s/c}} \boldsymbol{r}. \tag{22}$$

Although this model only approximates actual solar radiation pressure disturbances, it is sufficient for the purposes of this analysis in testing MPC robustness to disturbances.

3.5. Control disturbances

Mismatches and errors in control law actuation can be caused by a variety of factors. For example, improper deployment of the spacecraft from its launch vehicle can accidentally knock thruster nozzles off-axis. Misfires, sticking valves, or thruster malfunction can cause deviations from nominal thrust magnitudes. Imperfect nutation damping and attitude control can create additional thrust angle perturbations. Manufacturing tolerances contribute an additional (albeit small) source of uncertainty. Control actuation errors are especially likely to develop in systems that operate over long periods and thus may be particularly problematic for electric propulsion systems and other low thrust spacecraft. Without routine and systematic feedback, it can be costly to compensate for these errors at the end of the trajectory. See a related discussion of thrust errors on orbital transfers in [24]. To model this wide range of possible control disturbances, perturbed trajectories in the following section were simulated using a constant percentage thrust magnitude offset, T_{offset}, and a 1-σ thrust angle uncertainty, σ_{α_T}. For a constant thrust offset, the actual implemented thrust magnitude becomes

$$T_{\text{actual}} = T_{\text{nominal}}\left(1 + \frac{T_{\text{offset}}}{100}\right), \tag{23}$$

DOI: 10.1002/oca

and for actual implemented thrust angles, a pseudorandom selection was made from a normal distribution on the basis of the nominal commanded thrust angle and assumed standard deviation, σ_{α_T}.

4. NUMERICAL RESULTS

The MPC strategies described previously are applied to an Earth-to-Mars rendezvous OCP. Each is applied to the same orbital rendezvous scenario, with variations only in the MPC strategy used, the type of cost functional, and the propulsion model. All cases leave the end time unfixed. Table A.1 in the Appendix summarizes the input parameters of the problem scenario. The parameter values reflect those in Bryson [25].

Three test cases are examined as a baseline for evaluation of the proposed MPC strategies:

(1) Nuclear-electric propulsion, constant thrust magnitude, $T^* = T_0 = 0.5$ N, and minimum-time OCP.
(2) Nuclear-electric propulsion, variable thrust magnitude $0 \leqslant T(t) \leqslant T_{\max} = 0.5$ N, and minimum-fuel OCP.
(3) Solar-electric propulsion and minimum-fuel OCP (with $T_0 = 0.5$ N at 1 AU).

Numerical results of two MPC strategies, CNCN and SNNS (as described in Section 2.3), are given. Both are compared with the open-loop optimal control trajectory of test case (1) to illustrate the magnitude of the error that the trajectory designer would normally need to overcome using a TCM. Then, only the better of the two in terms of its performance (computation time,[§] robustness, and handling of orbital perturbations and disturbances) is tested against cases (2) and (3). All test cases examine both an unperturbed case, in which both the predictive model and the model used for simulation were exactly alike, and a perturbed case, in which the predictive model neglected to include the orbital perturbations and control disturbances outlined in the previous section. In particular, for the control disturbances, a constant thrust offset T_{offset} of -10% and a normally distributed thrust angle with σ_{α_T} of 3° was studied. This thrust angle uncertainty is consistent with typical electric propulsion thrusters such as the Russian SPT-140 as used in [26], which assumes 1° direction uncertainty.

All simulations utilize unit scaling, with astronomical units (AU) for position and the earth days for time. The open-source optimization program ACADO toolkit (an acronym for automatic control and dynamic optimization), developed by David Ariens *et al.*, was used as the optimizer.[¶] This software was chosen for its accessibility, robust numerical convergence, and convenient interface with MATLAB [27]. A direct multiple-shooting method, using sequential quadratic programming with full Broyden–Fletcher–Goldfarb–Shanno Hessian updates, was employed for each analysis. A fourth-order Runge–Kutta integrator was used for numerical integration.

4.1. Nuclear-electric, constant thrust case

Here, the results for the first OCP test case are presented. Because the thrust is constrained to a constant value, only the optimal thrust angle trajectory is required to solve the OCP. The open-loop control, CNCN MPC, and SNNS MPC strategies are each applied, and their performance is compared.

4.1.1. Open-loop control. Figures 3 and 4 show the optimal open-loop solutions to the minimum-time OCP for $T = 0.5$ N and for $N = 30$ control subintervals. The thrust angle is defined in the spacecraft local-vertical–local-horizontal frame, with a value of 0° aligning the thrust vector with the local vertical, away from the sun (see Figure 2).

[§]Computation times are reported as the maximum fraction of time required per sampling period (over all sampling periods). For the open-loop case, this is just the computation time over the total horizon. This fraction includes the time required to reformulate the optimal control problem and run the optimizer but does not include compiling time. Simulations were run on a 32-bit machine with 3.49 GB usable RAM and a 3.06 GHz dual-core processor.
[¶]http://www.acadotoolkit.org/

DOI: 10.1002/oca

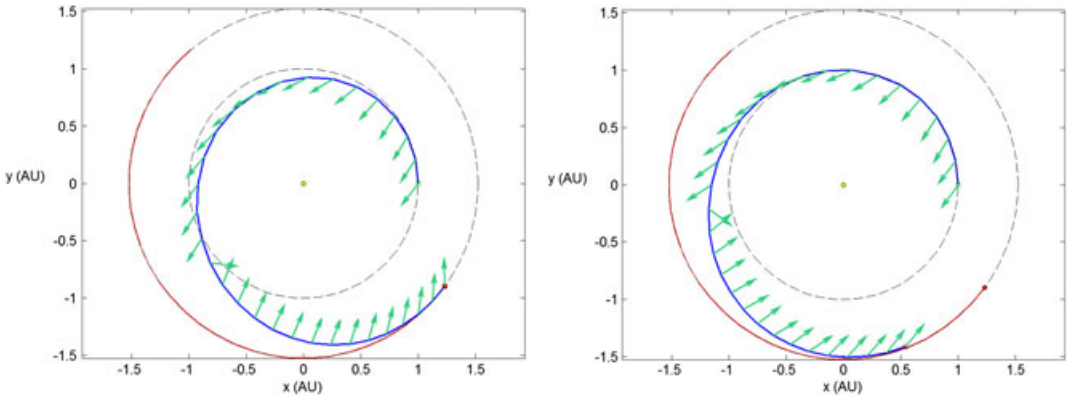

Figure 3. Optimal open-loop spacecraft trajectories simulated both without (left) and with (right) orbital perturbations included ($t_f^* = 370.2901$ days). Arrows point in the thrust direction.

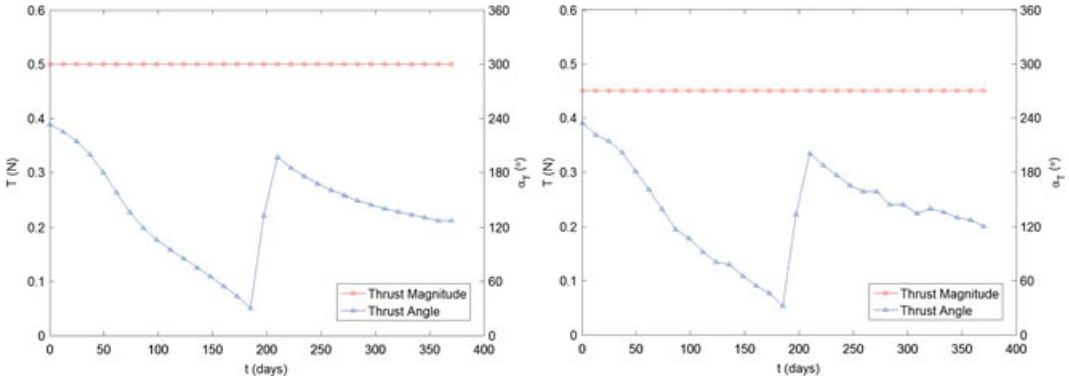

Figure 4. Optimal open-loop thrust magnitude and thrust angle histories for the unperturbed (left) and perturbed (right, with uncertainties added) cases.

The open-loop trajectory performs well when the equations of motion accurately describe the spacecraft on its mission; however, in the case that there are perturbations or control law disturbances that are unknown or inaccurately represented in the OCP, following the open-loop trajectory unsurprisingly produces significant errors. In this case, the spacecraft fails to rendezvous with Mars when gravitational effects from Earth and Mars, solar radiation pressure, a –10% thrust magnitude offset, and 3° thrust angle uncertainty are not modeled. For the perturbed trajectory shown, the spacecraft has a terminal position error magnitude of 0.8685 AU and a terminal velocity error magnitude of 0.8224 km/s.

4.1.2. CNCN MPC closed-loop control. Figures 5–7 show the closed-loop solutions derived from the CNCN MPC control framework. A constant $N = 30$ control subintervals were used for the OCP planning period considered at each time instant.

As can be seen in Figure 5, the CNCN MPC strategy is successful in rendezvousing with the target, both with and without the presence of perturbations and control law disturbances. Note that there is an interesting difference between the CNCN and open-loop results: the CNCN strategy achieves convergence in a slightly longer time than the open-loop control. See Figure 6, which shows that the control becomes erratic, particularly with perturbations included. The irregularities seen in the thrust angle near the end of the trajectory are indicative of the fine-tune trajectory adjustments the spacecraft is attempting to make to improve its convergence to the target planet. From Figure 7, the CNCN method results in small positional and velocity errors in relation to the target planet, even when disturbances unknown to the spacecraft are present and fairly significant. This comes at the

DOI: 10.1002/oca

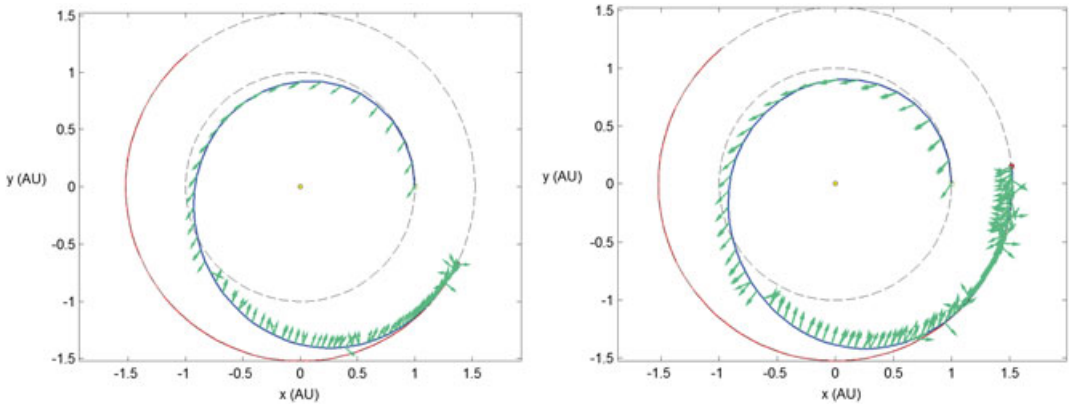

Figure 5. Closed-loop CNCN MPC trajectories simulated both without (left) and with (right) orbital perturbations included ($t_f^* = 389.5172$ days, 449.8818 days). Arrows point in the thrust direction; two arrows at the same point indicate an instantaneous jump in thrust direction.

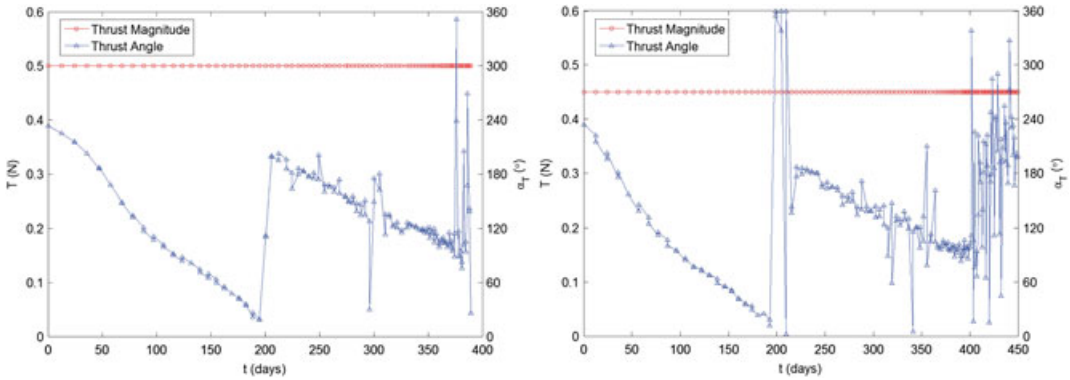

Figure 6. CNCN MPC thrust and thrust angle histories for the unperturbed (left) and perturbed (right) cases.

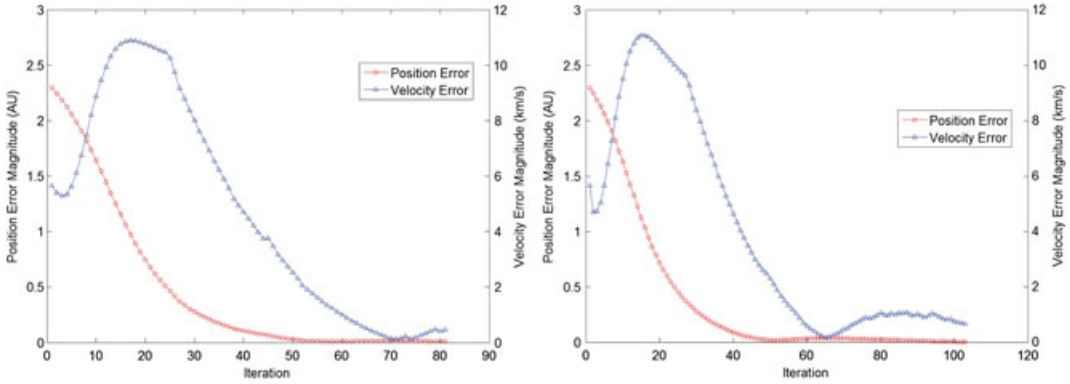

Figure 7. CNCN MPC position and velocity error magnitudes (2-norms) as a function of iteration for the unperturbed (left) and perturbed (right) trajectories.

cost, however, of reevaluating the OCP 80 times in the unperturbed case and over 100 times in the perturbed case.

4.1.3. SNNS MPC closed-loop control. Figures 8–10 show the optimal closed-loop solutions derived from the SNNS MPC control framework. The optimization routine was also initialized with $N = 30$ control subintervals.

DOI: 10.1002/oca

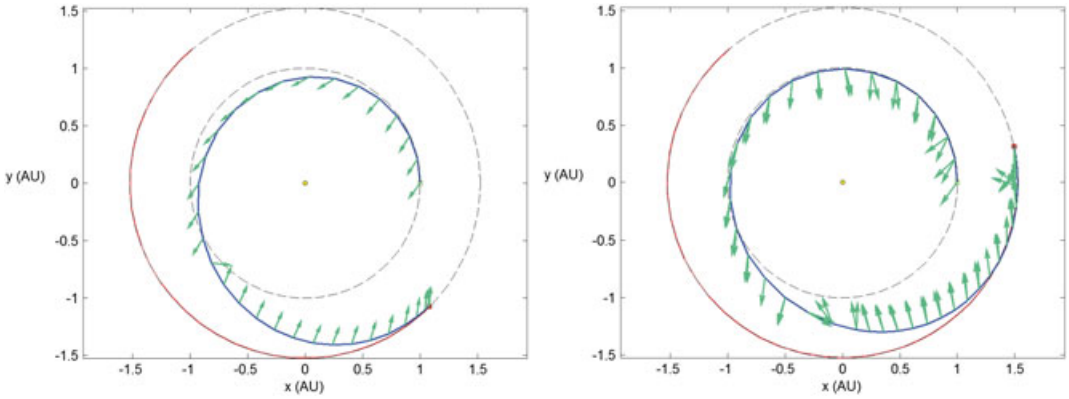

Figure 8. Closed-loop SNNS MPC trajectories simulated both without (left) and with (right) orbital perturbations included ($t_f^* = 353.3658$ days, 461.6004 days). Arrows point in the thrust direction; two arrows at the same point indicate an instantaneous jump in thrust direction.

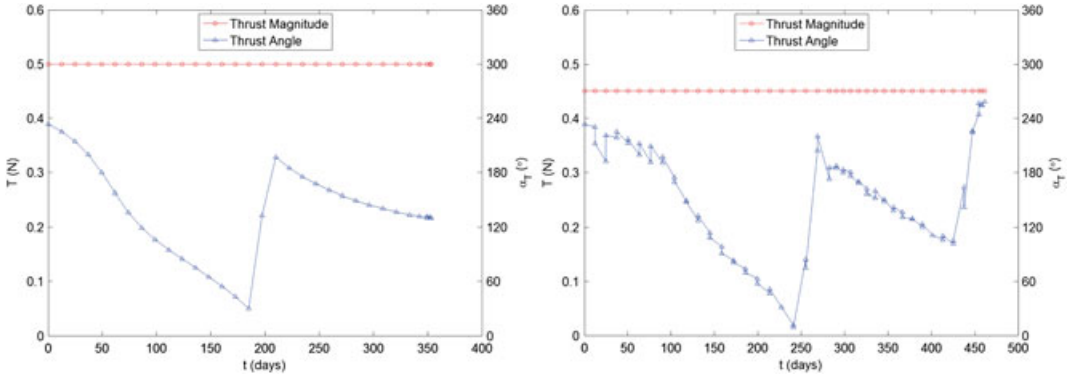

Figure 9. SNNS MPC thrust and thrust angle histories for the unperturbed (left) and perturbed (right) cases.

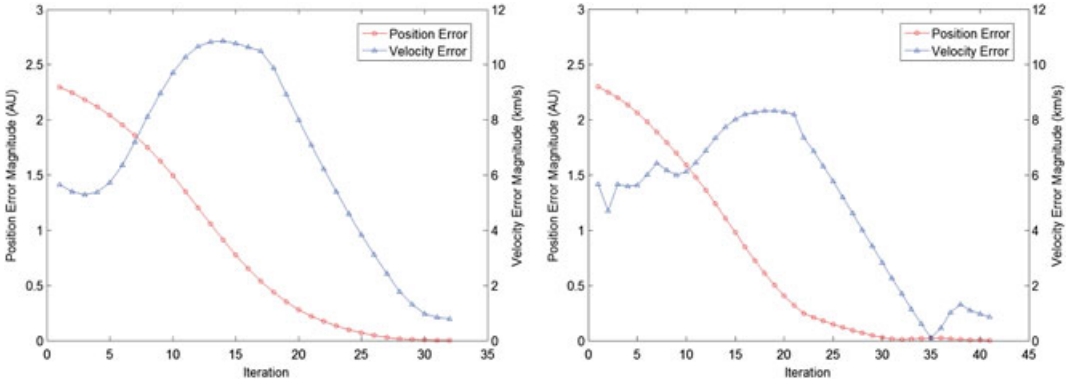

Figure 10. SNNS MPC position and velocity error magnitudes (2-norms) as a function of iteration for the unperturbed (left) and perturbed (right) trajectories.

First, from the left plots of Figures 8 and 9, noting that the SNNS unperturbed control is virtually identical to the open-loop control, it can be seen that the open-loop trajectory is approximately recovered when disturbances are absent. Furthermore, it is observed that with the SNNS strategy, as with the CNCN strategy, reevaluation of the minimum-time control problem along the trajectory compensates for the perturbations and disturbances, despite the fact that they are never modeled in the equations of motion. Subdivisions, or doubling of the number of control nodes, were made at planning periods 30 and 31 for the unperturbed trajectory and at planning periods 22 and 39 for the

DOI: 10.1002/oca

Table I. Performance comparison among the open-loop and closed-loop control strategies for the nuclear-electric constant thrust Earth-to-Mars rendezvous problem.

	Unperturbed EOM's			Perturbed EOM's		
	Open-loop	CNCN	SNNS	Open-loop	CNCN	SNNS
Converged to Mars?	Yes	Yes	Yes	No	Yes	Yes
$J = t_f - t_0$ (days)	370.29	389.52	353.37	N/A	449.88	461.60
Max. comp. time/subinterval	$3.934{\cdot}10^{-7}$	$1.043{\cdot}10^{-4}$	$5.999{\cdot}10^{-5}$	N/A	$1.111{\cdot}10^{-4}$	$1.127{\cdot}10^{-4}$
Fuel cost, $m_0 - m_f$ (kg)	543.74	571.97	518.89	N/A	660.61	677.82

N/A indicates failure to compute the maneuver. EOM's, equations of motion; Max. comp. time/subinterval is the maximum time to compute the next control per subinterval, over all subintervals; CNCN, constant number of control nodes; SNNS, shrinking number of nodes with subdivision.

perturbed trajectory. Without orbital perturbations or disturbances, the SNNS thrust angle feedback control managed to achieve rendezvous with Mars 16.92 days faster than the open-loop thrust angle control law. At first glance, this may seem counterintuitive, in that the maneuver time for the unperturbed SNNS MPC trajectory is shorter than the 'ideal' open-loop trajectory. This is likely due to the two subdivisions made over the course of the MPC trajectory, allowing for more finely-timed control adjustments and therefore a slightly faster rendezvous. With disturbances present, feedback enabled convergence to Mars after 461.6 days, easily overcoming all of the errors inherent to the open-loop method. See Table I for a comparison of major results.

4.1.4. Comparison of control strategies. A comparison is made in Table I between the open-loop, CNCN closed-loop, and SNNS closed-loop solutions to the minimum-time, nuclear-electric propulsion, $T \equiv 0.5$ N Earth-to-Mars rendezvous problem. Performance was evaluated on the basis of the ability to converge to the target, computational times, and optimal cost functional values.

It is evident that, with the open-loop control, the spacecraft has little chance of reaching Mars when there are significant real-world perturbations and disturbances that are unaccounted for in the OCP formulation. In contrast, both MPC frameworks were able to overcome these unmodeled influences through systematic reevaluation of the minimum-time OCP along the trajectory. Although it may in reality be more realistic to use higher-fidelity models in such rendezvous scenarios, the goal of this paper was to investigate whether or not feedback introduced through MPC could overcome such modeling inaccuracies, disturbances, and control actuation errors. Convergence to Mars even in the face of such significant disturbances substantiates the method, revealing that even in the worst cases, these nonlinear strategies can work well provided sufficient time is available to update the solution. This suggests that nonlinear MPC for low thrust spacecraft trajectory control can overcome substantial errors and sudden or uncertain changes during a mission, perhaps even mission-critical failures that offset the thrust or thrust angles rather significantly.

On the other hand, as can be seen in Table I, the MPC techniques involve significantly more computational effort than a single open-loop iteration (although still only requiring on the order of 0.01% of the time available, as indicated by the maximum computational time required per subinterval to compute the next control over all subintervals). This is a result of the fact that many additional reevaluations of the OCP are needed to provide a 'sampling frequency' sufficiently high to counteract disturbances. The CNCN MPC framework increases this frequency as the simulation progresses by holding the number of control nodes constant, yet this means that there are diminishing returns in calculation time as the spacecraft approaches the target because the duration of the maneuver shrinks, and only the first control segment is implemented from iteration to iteration. SNNS MPC strategy overcomes this problem, yet each iteration requires twice as many evaluations of the OCP as CNCN because it checks during each iteration whether doubling the number of control nodes is beneficial. Without perturbations, SNNS yields a shorter computation time versus the CNCN technique not only due to its ability to initialize the next planning period by using results from the previous planning period, but also because of its reduction in problem complexity as the number of control intervals shrinks from iteration to iteration. With comparable fuel consumptions and final times, this advantage of SNNS over CNCN distinguishes SNNS as the favorable MPC strategy for the

DOI: 10.1002/oca

orbital rendezvous problem considered in this paper. The SNNS MPC method is therefore chosen for evaluation against open-loop control for the remaining two test cases.

4.2. Additional cases

To briefly demonstrate the ability of the SNNS MPC strategy to handle more difficult scenarios, the optimal closed-loop trajectories for two 'minimum-fuel' Earth-to-Mars rendezvous OCP's are given, the first for a nuclear-electric propulsion system with bounded thrust and the second for a solar-electric spacecraft. Numerical results are summarized in Section 4.3, which follows.

4.2.1. Nuclear-electric, bounded thrust case. Figures 11 and 12 show the SNNS MPC closed-loop solutions for thrust bounded to less than 0.5 N. Again, the SNNS strategy leads to convergence with the target, regardless of the presence of disturbances.

4.2.2. Solar-electric case. Figures 13 and 14 present the SNNS optimal closed-loop solutions for a solar-electric spacecraft with state-dependent thrust constraints, which also show successful convergence to the target by using the SNNS technique.

4.3. Comparison of SNNS control strategy test cases.

A summary of major numerical results from the SNNS control strategy for each test scenario is shown in Table II.

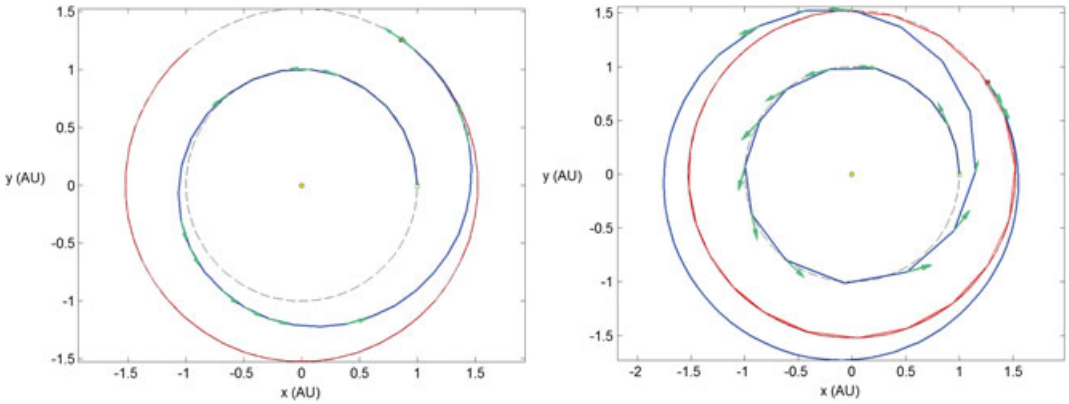

Figure 11. Closed-loop nuclear-electric, bounded-thrust SNNS MPC trajectories simulated both without (left) and with (right) orbital perturbations included ($t_f^* = 544.9372$ days, 1190.9719 days). Arrows point in the thrust direction; two arrows at the same point indicate an instantaneous jump in thrust direction.

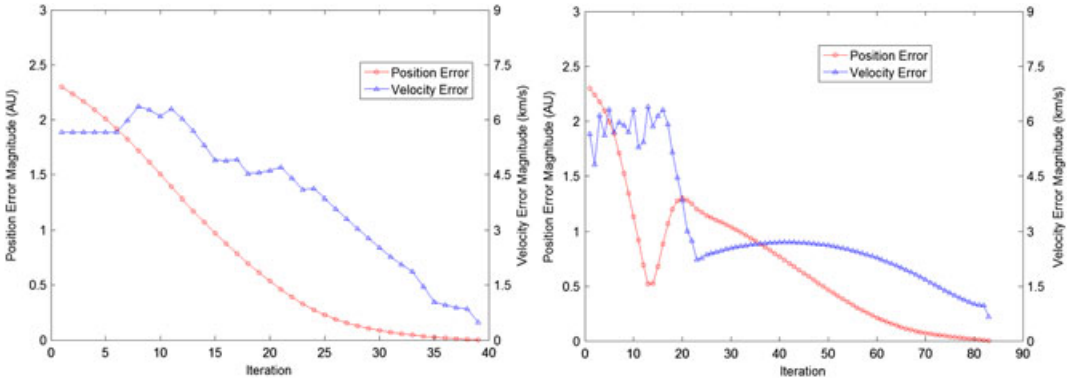

Figure 12. Nuclear-electric, bounded-thrust SNNS MPC position and velocity error magnitudes (2-norms) as a function of iteration for the unperturbed (left) and perturbed (right) trajectories.

DOI: 10.1002/oca

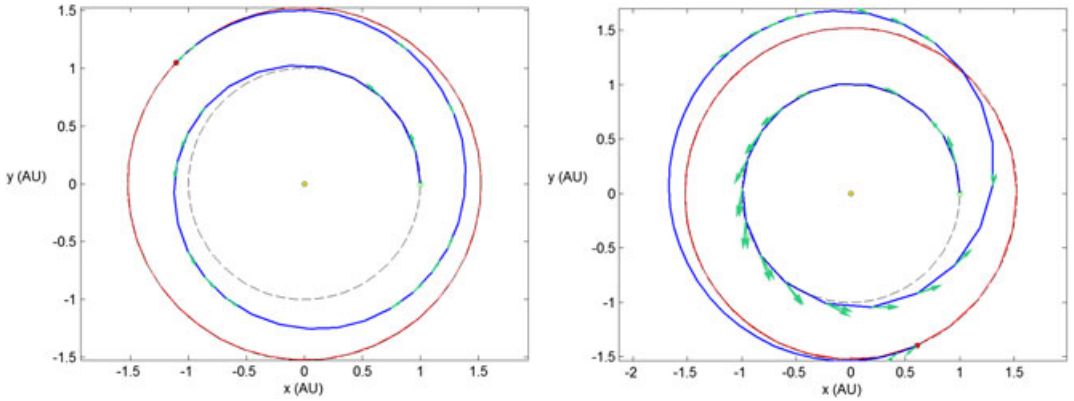

Figure 13. Closed-loop solar-electric SNNS MPC trajectories simulated both without (left) and with (right) orbital perturbations included ($t_f^* = 699.4135$ days, 999.2534 days). Arrows point in the thrust direction; two arrows at the same point indicate an instantaneous jump in thrust direction.

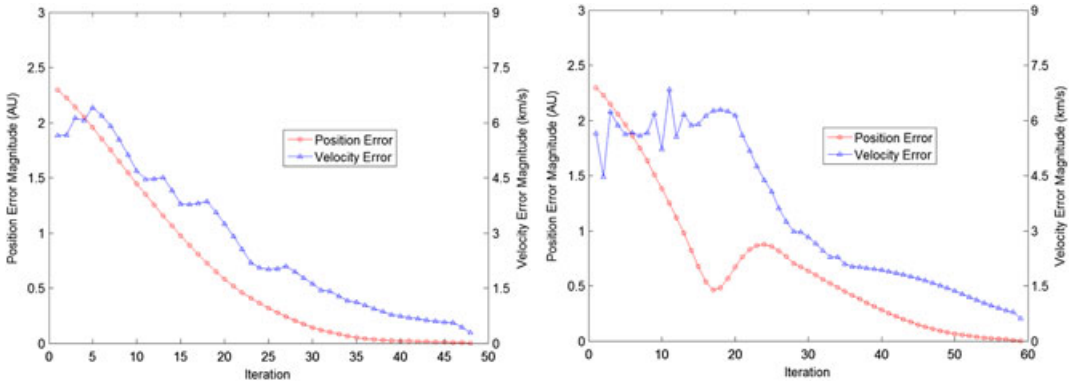

Figure 14. Solar-electric SNNS MPC position and velocity error magnitudes (2-norms) as a function of iteration for the unperturbed (left) and perturbed (right) trajectories.

Table II. Performance comparison among test cases for the SNNS MPC closed-loop control strategy for the minimum-fuel Earth-to-Mars rendezvous problem.

	Unperturbed EOM's			Perturbed EOM's		
	Nuclear-electric, constant thrust	Nuclear-electric, bounded thrust	Solar-electric	Nuclear-electric, constant thrust	Nuclear-electric, bounded thrust	Solar-electric
Converged to Mars?	Yes	Yes	Yes	Yes	Yes	Yes
$t_f - t_0$ (days)	353.37	544.94	699.41	461.60	1090.97	999.25
$J = m_0 - m_f$ (kg)	518.89	240.75	217.46	677.82	465.82	359.30

EOM's, equations of motion.

5. CONCLUSION

In this paper, it is demonstrated that feedback using MPC can successfully complete an Earth-to-Mars rendezvous starting from the edge of Earth's sphere of influence using either a nuclear-electric or solar-electric spacecraft. A minimum-time OCP for a constant thrust nuclear-electric

DOI: 10.1002/oca

spacecraft was used for comparison of the CNCN and SNNS MPC strategies with open-loop optimal control. A minimum-fuel OCP for a bounded thrust nuclear-electric spacecraft and a minimum-fuel OCP for a solar-electric spacecraft were also successfully handled by the SNNS MPC technique. Convergence to Mars was achieved under perturbations and control disturbances within reasonable times relative to the unperturbed optimal control trajectory and with marginal increases in fuel expenditure. It was shown that the effects of gravitational perturbations due to Earth and Mars, solar radiation pressure, a -10% constant negative thrust offset, and 3° thrust angle uncertainty were overcome and did not result in a loss of controllability and convergence for either of the MPC control schemes.

Model predictive control appears to be a viable technique for introducing feedback into low thrust orbital transfer problems. The MPC approach, involving systematic reevaluation of the OCP, has been shown to be effective at mitigating the growth of trajectory errors from the long-duration influence of unmodeled orbital perturbations and disturbances. The computational cost associated with doing so is an increase in computing time; however, relative to the time allotted for planning, computation times are still negligibly small (on the order of 10^{-4} percent), and therefore, the MPC techniques considered here appear to be adequate for on-board, real-time computations. Alternatively, the solutions may be computed off-board and uplinked to the spacecraft. Numerical convergence is greatly improved by initializing the optimal control algorithm at each iteration with results from the previous iteration. Results confirm that the SNNS framework, which takes advantage of this reinitialization, is better suited than the CNCN framework for the implementation of MPC strategies.

In the paper, it has been demonstrated that feedback solutions for interplanetary travel with good robustness properties can be developed on the basis of a specific formulation of MPC. An alternative approach, which also avoids ad hoc corrections, is to use conventional feedback to stabilize to an open-loop trajectory precomputed using optimal control techniques. The rigorous comparison of the two approaches in terms of performance and robustness, while addressing the stringent control constraints of low thrust actuation (that conventional feedback strategies are typically not well-equipped to handle), is beyond the scope of the present paper. It is interesting to note that little existing literature can be found that advocates this alternative approach for interplanetary missions. An exception is [28], which uses LQ-based strategies (although the method appears to be resilient only to disturbances in initial conditions). See also [3] for a different, Lyapunov-based approach to developing feedback solutions for orbital transfers (which does not, however, treat the rendezvous problem).

Stability and feasibility conditions for the usual MPC formulation, often involving terminal state/set conditions or terminal penalties, are considered, for example, in [5, 6, 15]. In this paper, a simple stability analysis was presented for the constant thrust, minimum-time MPC formulation; although their stability was not formally proven here, correspondingly stable formulations of MPC involving terminal state constraints were also developed for the minimum-fuel cases as well. A more rigorous analysis of conditions for stability and recursive feasibility that accounts for different features of the computational strategies introduced in this work will be reported elsewhere.

Opportunity for further work includes the applicability of MPC strategies to longer-duration interplanetary maneuvers, noncoplanar orbital transfer problems, solar sail propulsion models, and other low thrust trajectory optimization problems. Because the long maneuver times required, we expect that these more complex cases of orbital transfer can be handled computationally without many complications; however, we leave the details to future work. It is also of interest to investigate the convergence of an MPC control scheme that implements more than one control subinterval between iterations and before reformulation of a new planning period, otherwise called ‘block-MPC’ strategies. These have the potential to reduce computational effort and time further. Finally, one of the interesting observations of this research is that MPC may be able to allow the trajectory designer to intentionally neglect higher-order modeling terms, relying instead on feedback to compensate for potential errors. Solving the simpler problem repeatedly may more easily generate an optimal trajectory in comparison with solving the higher-order, high-fidelity OCP only once. Further investigation is needed to test this concept.

DOI: 10.1002/oca

APPENDIX

Table A.1. List of input parameters by category.

Problem definition		
t_0	Starting time of simulation	0 days
r_E	Radius of Earth's orbit about the sun	149597871 km
r_M	Radius of Mars' orbit about the sun	227939100 km
m_E	Mass of Earth	5.9736×10^{24} kg
m_M	Mass of Mars	6.4191×10^{23} kg
m_S	Mass of the sun	1.98892×10^{30} kg
μ	Gravitational parameter for the sun	132712440018 km^3/s^2
Spacecraft initial conditions		
r_0	Spacecraft initial radius	149597871 km
θ_0	Spacecraft initial heliocentric polar angle	0°
$(v_r)_0$	Spacecraft initial radial velocity	0 km/s
$(v_\theta)_0$	Spacecraft initial circumferential velocity	29.78469 km/s
m_0	Spacecraft initial total mass	1500 kg
Target planet initial conditions		
$(r_T)_0$	Mars initial radius	227939100 km
$(\theta_T)_0$	Mars initial heliocentric polar angle	130°
$(v_{r,T})_0$	Mars initial radial velocity	0 km/s
$(v_{\theta,T})_0$	Mars initial circumferential velocity	24.12939 km/s
Perturbation inputs		
$A_{s/c}$	Planform area of spacecraft with respect to sun–spacecraft line	50 m^2
η	Reflectivity efficiency of spacecraft	0.6
S_0	Solar constant (solar intensity at r = 1 AU)	1368 W/m^2
c	Speed of light in vacuum	299792458 m/s
T_{offset}	Value of constant thrust offset	–10%
σ_{α_T}	1-σ uncertainty in thrust angle actuation	3°
μ_E	Gravitational parameter for Earth	398600.441 km^3/s^2
μ_M	Gravitational parameter for Mars	42828 km^3/s^2
$(\theta_E)_0$	Initial angular position of Earth	–0.35414°
Propulsion model parameters		
Nuclear-electric		
I_{sp}	Specific impulse	3000 s
g_0	Standard gravitational acceleration	9.80655 m/s^2
Solar-electric		
a_1	Engine-specific constant parameter	1.1063
a_2	Engine-specific constant parameter	0.1495
a_3	Engine-specific constant parameter	–0.2990
a_4	Engine-specific constant parameter	–0.0423
b_1	Engine-specific constant parameter	–1.9137
b_2	Engine-specific constant parameter	36.2429
c_1	Engine-specific constant parameter	–0.4756
c_2	Engine-specific constant parameter	–0.9021
Convergence criteria		
$(r_{SOI})_E$	Radius of sphere of influence of Earth	9.24641×10^5 km
$(r_{SOI})_M$	Radius of sphere of influence of Mars	5.77247×10^5 km

ACKNOWLEDGMENT

The authors would like to thank N. Harris McClamroch of the University of Michigan for his numerous suggestions and contributions to the research contained in this paper.

DOI: 10.1002/oca

REFERENCES

1. Conway BA. *Spacecraft Trajectory Optimization*, (1st edn). Cambridge University Press, New York: NY, 2010.
2. Dankanich JW. Electric propulsion for small body missions. *46th AIAA/ASME/SAE/ASEE Joint Propulsion Conference & Exhibit*, Nashville Convention Center and Renaissance Nashville Hotel, Nashville, TN (United States), 2010.
3. Chang DE, Chichka DF, Marsden JE. Lyapunov-based transfer between elliptic keplerian orbits. *Discrete and Continuous Dynamical Systems – Series B* 2002; **2**(1):57–67. DOI: 10.3934/dcdsb.2002.2.57.
4. Starek JA, Kolmanovsky IV. Model predictive feedback control strategy for low thrust spacecraft interplanetary missions. *Advances in the Astronautical Sciences Series* 2011; **140**:1879–1898.
5. Maciejowski JM. *Predictive Control with Constraints*, (1st edn). Pearson Education: Upper Saddle River, New Jersey, 2002.
6. Camacho E, Bordons Alba C. *Model Predictive Control*, (2nd edn). Springer: New York City, New York, 2007.
7. Park H, Di Cairano S, Kolmanovsky IV. Model predictive control for spacecraft rendezvous and docking with a rotating/tumbling platform and for debris avoidance. *International Journal of Robust and Nonlinear Control* 2012. DOI: 10.1002/rnc.2827.
8. Richards AG. Robust constrained model predictive control. *Ph.D. Dissertation*, Massachusetts Institute of Technology, Cambridge: MA, 2005. URI: 1721.1/28914.
9. Breger LS. Control of spacecraft in proximity orbits. *Ph.D. Dissertation*, Massachusetts Institute of Technology, Cambridge: MA, June 2007. URI: 1721.1/40390.
10. Richards AG, How JP. Model predictive control of vehicle maneuvers with guaranteed completion time and robust feasibility. *Proceedings of the 2003 American Control Conference*, Denver: CO, 2003; **5**:4034–4040. DOI: 10.1109/ACC.2003.1240467.
11. Arrieta-Camacho JJ, Biegler LT. Real time optimal guidance of low-thrust spacecraft: an application of nonlinear model predictive control. *Annals of the New York Academy of Sciences* 2005; **1065**:174–188. DOI: 10.1196/annals.1370.001.
12. Gao Y. Low-thrust nonlinear guidance by tracking mean orbital elements. *Journal of Guidance, Control, and Dynamics* 2008; **31**(3):1103–1110. DOI: 10.2514/1.31256.
13. Losa D. High vs low-thrust station keeping maneuver planning for geostationary satellites. *Ph.D. Dissertation*, Ecole Nationale Superieure des Mines de Paris, Paris: France, 2007.
14. Huang R, Hwang I, Corless M. A new nonlinear model predictive control algorithm using differential transformation with application to interplanetary low-thrust trajectory tracking. *Proceedings of the 2009 American Control Conference*, Hyatt Regency, St. Louis Riverfront, St. Louis, Missouri (United States), 2009; 4868–4873, DOI: 10.1109/ACC.2009.5160555.
15. Mayne DQ, Rawlings JB, Rao CV, Scokaert POM. Constrained model predictive control: stability and optimality. *Automatica* 2000; **36**:789–814. DOI: 10.1016/S0005-1098(99)00214-9.
16. Camacho E, Bordons C. Nonlinear model predictive control: an introductory review. In *Assessment and Future Directions of Nonlinear Model Predictive Control*. Springer, Berlin: Germany, 2007; 1–16. DOI: 10.1007/978-3-540-72699-9_1.
17. Larson WJ, Wertz JR. *Space Mission Analysis and Design*, (2nd edn). Microcosm Inc., Torrance: CA, 1992; 644.
18. Wie B. *Space Vehicle Dynamics and Control*, (2nd edn). AIAA Education Series, AIAA Inc.: VA, 1998; 291.
19. Bryson AE, Ho YC. *Applied Optimal Control: Optimization, Estimation, and Control*. Taylor & Francis, Abingdon: UK, 1975; 134.
20. Kim M. Continuous Low-thrust Trajectory Optimization: Techniques and Applications. *Ph.D. Dissertation*, Aerospace Engineering Dept., Virginia Polytechnic and State University, Blacksburg: VA, 2005.
21. Williams SN, Coverstone-Carroll VL. Benefits of solar electric propulsion for the next generation of planetary exploration missions. *The Journal of Astronautical Sciences* 1997; **45**(2):143–160.
22. Vallado DA, McClain WD. *Fundamentals of Astrodynamics and Applications*, (2nd edn). Microcosm Press, El Segundo: CA, 2001; 135.
23. Dachwald B. Low-thrust trajectory optimization and interplanetary mission analysis using evolutionary neurocontrol. *Ph.D. Dissertation*, Universitat der Bundeswehr Munchen, Neubiberg: Germany, 2004.
24. Sidi MJ. *Spacecraft Dynamics and Control: A Practical Engineering Approach*. Cambridge University Press: Cambridge, England, 1997; 84.
25. Bryson AE. *Dynamic Optimization*. Prentice-Hall: Upper Saddle River, NJ, 1999; 126–130.
26. Akim EL, Zaslavsky GS, Zharov VG, Chernov AV. Interplanetary flight control with electric engine in view of thrust errors. *Proceedings of 18th International Symposium on Space Flight Dynamics (ESA SP-548)*, ADS, Munich: Germany, 2004; 339–343.
27. Ariens D, Houska B, Ferreau H, Logist F. ACADO for Matlab User's Manual. In *Optimization in Engineering Center (OPTEC)*, 1.0 beta ed., 2010.
28. Owis A, Topputo F, Bernelli-Zazzera F. Feedback optimal control in low-thrust interplanetary trajectory design. *12th International Conference on Aerospace Sciences & Aviation Tech.*, Military Technical College, Cairo: Egypt, 2007.